IOPscience iopscience.iop.org

Home Search Collections Journals About Contact us My IOPscience

Calculation of Auger electron diffraction at a Ni(111) surface

This article has been downloaded from IOPscience. Please scroll down to see the full text article.

1990 J. Phys.: Condens. Matter 2 9735

(http://iopscience.iop.org/0953-8984/2/49/002)

View the table of contents for this issue, or go to the journal homepage for more

Download details:
IP Address: 171.66.16.151
The article was downloaded on 11/05/2010 at 07:02

Please note that terms and conditions apply.

J. Phys.: Condens. Matter **2** (1990) 9735–9747. Printed in the UK

Calculation of Auger electron diffraction at a Ni(111) surface

V Fritzsche

Sektion Physik der Technischen Universität Dresden, Mommsenstrasse 13, DDR-8027 Dresden, Federal Republic of Germany

Received 28 March 1990, in final form 11 July 1990

Abstract. A new formalism for the calculation of elastic multiple-scattering processes of electrons is presented, which takes the spherical character of the electron waves fully into account. It is based on a magnetic quantum number expansion of the electron Green's function and makes extensive use of recurrence relations. In the present paper this method is applied to the escaping electron in the final state of Auger electron spectroscopy (AES). Formulae for an analytic integration of the electron intensity over the aperture of the detector are derived and inserted into this calculation scheme. Within this framework angle-resolved $M_{23}VV$ Auger electron intensities from a clean Ni(111) surface are calculated for the first time and compared with experimental data.

1. Introduction

From photoelectron spectroscopy it is well known that a lot of valuable information on the electronic and geometrical structure in the surface region can be obtained through angle-resolved investigations. Angle-resolved Auger electron spectroscopy (AES), however, has attracted considerably less interest although AES is a widely used technique in surface physics. The intrinsic drawback of AES that is responsible for this situation is certainly the complicated excitation process, which involves two electrons. Nevertheless it is clear that the essential origins of the angle-dependent structures observed in the spectra of monocrystalline samples are elastic scattering processes of the excited electrons at atoms surrounding the escaping path of the electrons from the emitter to the surface. Therefore the question arises of whether Auger electron diffraction can be used for investigations of surface geometry. For this purpose the measured spectra must be compared with theoretical intensity distributions of all possible structure models for the surface region.

Several methods for calculating elastic scattering effects in excited electron states are known from similar spectroscopies, such as EXAFS, XANES and photoelectron diffraction. In the early days of angle-resolved AES it was mainly the dynamical LEED theory, which makes use of the two-dimensional periodicity of the sample [1–6], that was applied in multiple-scattering calculations. Now, cluster calculations are preferred because

(i) they are better adapted to the local nature of the excitation and scattering processes and

(ii) they allow easy variation of the atomic positions, even in complicated systems.

0953-8984/90/499735 + 13 $03.50 © 1990 IOP Publishing Ltd

Multiple-scattering cluster calculations within the framework of a full partial wave expansion are rather time-consuming and expensive at energies above 30 eV due to the large number of angular momenta which must be included. Therefore several approximations are used in calculations of EXAFS, XANES, photoelectron diffraction and Auger electron diffraction. It is generally acknowledged that the accuracy of a simple plane-wave approximation (PWA) is sufficient only for backscattering processes (single-scattering contributions in EXAFS) and to a lesser extent also for the scattering of spherical waves with low angular momenta into other directions (first scattering process of the excited electrons in photoelectron diffraction or Auger electron diffraction) [7–10]. The PWA fails significantly for all multiple-scattering pathways which contain forward-scattering events. Therefore in the last decade several attempts have been made to develop improved calculation procedures or approximation schemes for spherical-wave scattering which are numerically much faster than the ordinary partial wave expansion and which allow a reliable accuracy for all multiple-scattering processes [9, 11–15].

In the present paper we describe a new version of a magnetic quantum number expansion for the electron Green's function in the multiple-scattering theory, which continues the basic idea of the reduced angular momentum expansion (RAME) [9, 14, 15] and the Taylor-series magnetic quantum number expansion (TSMQNE) of Barton and Shirley [11, 12]. We derive efficient recurrence relations for the coefficients which describe the expansion of an outgoing spherical electron wave around a new centre in an angular momentum representation. These exact expressions allow us to bypass a doubtful approximation made in the TSMQNE. In the present paper this magnetic quantum number expansion is used for a description of the final state of Auger electrons, but unreservedly it can be applied also to photoelectron diffraction, x-ray absorption fine structures (XANES and EXAFS) or other related spectroscopies. As a further refinement the electron intensity is integrated over the aperture of the detector analytically.

In section 3 angle-resolved $M_{23}VV$ Auger electron spectra of Ni(111), which were calculated within this framework, are presented and compared with experimental data [16] for the main azimuths and different energies.

2. Theory

2.1. Multiple-scattering description of the final state in AES

In a first-order perturbation theory the angle-resolved Auger electron intensity is given by

$$I(\boldsymbol{K}, E) \sim \sum_{\boldsymbol{R}_0} \sum_{m_0} \left| \sum_{l_0} M_{L_0}(E) B_{L_0}(\boldsymbol{k}, \boldsymbol{R}_0) \right|^2 \tag{1}$$

where $\boldsymbol{K}$ is the wavevector of the plane waves describing the electrons far away from the sample and $\boldsymbol{k}$ is the corresponding wavevector inside the sample. The relationship between $\boldsymbol{K}$ and $\boldsymbol{k}$ is determined by the refraction effect at the surface potential step. The vector $\boldsymbol{R}_0$ denotes the diverse emitter positions and $M_{L_0}(E)$ contains the matrix elements for the Auger transitions from the considered initial state to all possible final states with the angular momenta $L_0 = (l_0, m_0)$ in which the escaping electron has the kinetic energy E. In our notation L is always an abbreviation for $L = (l, m)$.

The coefficients $B_{L_0}(\boldsymbol{k}, \boldsymbol{R}_0)$ describe the wavefunction of the excited electrons inside the sample:

$$B_{L_0}(\boldsymbol{k}, \boldsymbol{R}_0) = \mathrm{e}^{-\mathrm{i}\boldsymbol{k}\cdot\boldsymbol{R}_0} A^{(0)}_{L_0}(\boldsymbol{k}, \boldsymbol{R}_0) + \sum_{\boldsymbol{R}_1}{}' \mathrm{e}^{-\mathrm{i}\boldsymbol{k}\cdot\boldsymbol{R}_1} A^{(1)}_{L_0}(\boldsymbol{k}, \boldsymbol{R}_1, \boldsymbol{R}_0)$$
$$+ \sum_{\boldsymbol{R}_1}{}' \sum_{\boldsymbol{R}_2}{}' \mathrm{e}^{-\mathrm{i}\boldsymbol{k}\cdot\boldsymbol{R}_2} A^{(2)}_{L_0}(\boldsymbol{k}, \boldsymbol{R}_2, \boldsymbol{R}_1, \boldsymbol{R}_0) + \ldots . \tag{2}$$

The first term in (2) represents the direct wave and the following include single-, double- and higher-order-scattering contributions:

$$A^{(0)}_{L_0}(\boldsymbol{k}, \boldsymbol{R}_0) = \mathrm{i}^{-l_0} Y_{L_0}(\boldsymbol{k}) \tag{3}$$

$$A^{(1)}_{L_0}(\boldsymbol{k}, \boldsymbol{R}_1, \boldsymbol{R}_0) = \sum_{L_1} \mathrm{i}^{-l_1} Y_{L_1}(\boldsymbol{k}) T_{l_1}(\boldsymbol{R}_1) G_{L_1 L_0}(\boldsymbol{R}_1 - \boldsymbol{R}_0)$$

$$A^{(2)}_{L_0}(\boldsymbol{k}, \boldsymbol{R}_2, \boldsymbol{R}_1, \boldsymbol{R}_0) = \sum_{L_1} \sum_{L_2} \mathrm{i}^{-l_2} Y_{L_2}(\boldsymbol{k}) T_{l_2}(\boldsymbol{R}_2)$$
$$\times G_{L_2 L_1}(\boldsymbol{R}_2 - \boldsymbol{R}_1) T_{l_1}(\boldsymbol{R}_1) G_{L_1 L_0}(\boldsymbol{R}_1 - \boldsymbol{R}_0).$$

All terms containing an $\boldsymbol{R}_{i+1} = \boldsymbol{R}_i$ are excluded from the summations in (2). The $T_l(\boldsymbol{R}_j)$ are a function of the complex scattering phase shifts δ_l of the atom $\boldsymbol{R}_j$, which take into account thermal vibrations [17, 18],

$$T_l(\boldsymbol{R}_j) = \mathrm{i} \sin \delta_l \exp(\mathrm{i}\delta_l). \tag{4}$$

The coefficients

$$G_{L'L}(\boldsymbol{R}) = 4\pi \sum_{L''} \mathrm{i}^{l'-l+l''} h_{l''}(kR) Y^*_{L''}(\boldsymbol{R}) \int \mathrm{d}\Omega Y^*_{L'} Y_L Y_{L''} \tag{5}$$

in which $h_l(x) = h^{(1)}_l(x)$ are the spherical Hankel functions [19], describe the free electron propagator in an angular momentum representation. Using rotations of the coordinate system they may be replaced by coefficients $G_{L'L}(\boldsymbol{R}')$ with vectors $\boldsymbol{R}'$ lying on the positive z axis. We introduce a new symbol for these basic quantities in our formalism by

$$G_{L'L}(R\boldsymbol{e}_z) = g_{l'lm}(R)\delta_{m',m} \tag{6}$$

where $\boldsymbol{e}_z$ is the unity vector in the z direction. Now equations (3) become

$$A^{(0)}_{L_0}(\boldsymbol{k}, \boldsymbol{R}_0) = \mathrm{i}^{-l_0} \sqrt{(2l_0+1)/4\pi} D^{(l_0)}_{0m_0}(\boldsymbol{k}, \boldsymbol{e}_z)$$

$$A^{(1)}_{L_0}(\boldsymbol{k}, \boldsymbol{R}_1, \boldsymbol{R}_0) = \sum_{l_1} \sum_{q_1} \mathrm{i}^{-l_1} \sqrt{(2l_1+1)/4\pi} D^{(l_1)}_{0q_1}(\boldsymbol{k}, \boldsymbol{R}_{10})$$
$$\times T_{l_1}(\boldsymbol{R}_1) g_{l_1 l_0 q_1}(R_{10}) D^{(l_0)}_{q_1 m_0}(\boldsymbol{R}_{10}, \boldsymbol{e}_z)$$

$$A^{(2)}_{L_0}(\boldsymbol{k}, \boldsymbol{R}_2, \boldsymbol{R}_1, \boldsymbol{R}_0) = \sum_{l_2} \sum_{q_2} \sum_{l_1} \sum_{q_1} \mathrm{i}^{-l_2} \sqrt{(2l_2+1)/4\pi}$$
$$\times D^{(l_2)}_{0q_2}(\boldsymbol{k}, \boldsymbol{R}_{21}) T_{l_2}(\boldsymbol{R}_2) g_{l_2 l_1 q_2}(R_{21}) D^{(l_1)}_{q_2 q_1}(\boldsymbol{R}_{21}, \boldsymbol{R}_{10})$$
$$\times T_{l_1}(\boldsymbol{R}_1) g_{l_1 l_0 q_1}(R_{10}) D^{(l_0)}_{q_1 m_0}(\boldsymbol{R}_{10}, \boldsymbol{e}_z) \tag{7}$$

with $\boldsymbol{R}_{ij} = \boldsymbol{R}_i - \boldsymbol{R}_j$. The $D^{(l)}_{mm'}$ are rotation matrices, which are defined in the appendix, where appropriate recurrence relations can also be found.

In expression (7) the numerical effort of computing the wavefunction can be optimized by making use of the fact that the magnitude of the coefficients $g_{l'lm}(R)$ decreases systematically and considerably with ascending absolute value of the magnetic quantum number m. That means the sums over the magnetic quantum numbers q_i in (7) can be restricted to a narrow range $-M \leq q_i \leq M$ without any substantial loss of accuracy. In this way a lot of unimportant terms in (7) can be skipped in practical calculations. In the energy range up to 1000 eV values of $M = 1 \ldots 3$ are sufficient to limit the errors for scattering processes between nearest neighbours, which are the most unfavourable cases for such a truncation, to 1% or less. At these energies angular momenta up to $l_{\max} = 10 \ldots 20$ must be included in the partial wave expansion. Therefore a truncation of the q_i sums in (7) reduces the numerical work considerably in comparison with a calculation on the basis of equation (3), in which all m_i from the interval $-l_{\max} \leq -l_i \leq m_i \leq l_i \leq l_{\max}$ must be taken into account.

For the first time these properties of the quantities $g_{l'lm}(R)$ have been utilized in the reduced angular momentum expansion (RAME) [9, 20], where M was chosen to be 1 and the $g_{l'lm}(R)$ were approximated by simple expressions.

2.2. *Recurrence relations for the* $g_{l'lm}(R)$

The question of how to calculate the quantities $g_{l'lm}(R)$ is of essential importance for minimizing the computational effort. In this section it will be shown that the complete set of coefficients $g_{l'lm}(R)$ needed in (7) can be calculated by means of simple recurrence relations.

From equation (5) it follows immediately that

$$g_{l'lm}(R) = N_{l'm} N_{lm}\, \mathrm{i}^{l'-l} \times 2\pi \sum_{l''} \mathrm{i}^{l''}(2l''+1) h_{l''}(kR) \int_{-1}^{+1} \mathrm{d}\zeta\, P_{l'}^{m}(\zeta) P_{l}^{m}(\zeta) P_{l''}(\zeta) \tag{8}$$

with

$$N_{lm} = \left(\frac{2l+1}{4\pi} \frac{(l-m)!}{(l+m)!} \right)^{1/2} \tag{9}$$

where $P_l^m(\zeta)$ are the associated Legendre polynomials. The $g_{l'lm}(R)$ obey the symmetry relations

$$g_{l',l,m}(R) = g_{l',l,-m}(R) = (-1)^{l'+l} g_{l,l',m}(R) \tag{10}$$

which follow from (8) and

$$P_l^{-m}(x) = (-1)^m [(l-m)!/(l+m)!] P_l^m(x). \tag{11}$$

Therefore recurrence relations are needed only for the index range $m \geq 0$ and $l \geq l'$, in which, of course, the conditions $l \geq m$ and $l' \geq m$ must be fulfilled.

With the help of

$$(2l+1)x P_l^m(x) = (l-m+1)P_{l+1}^m(x) + (l+m)P_{l-1}^m(x) \tag{12}$$

one obtains from equation (8)

$$a_{l'+1,m}g_{l'+1,l,m}(R) = a_{l,m}g_{l',l-1,m}(R) - a_{l+1,m}g_{l',l+1,m}(R) + a_{l',m}g_{l'-1,l,m}(R) \tag{13}$$

and

$$a_{m+1,m}g_{m+1,l,m}(R) = a_{l,m}g_{m,l-1,m}(R) - a_{l+1,m}g_{m,l+1,m}(R) \tag{14}$$

with

$$a_{l,m} = \sqrt{(l^2 - m^2)/(4l^2 - 1)}. \tag{15}$$

Now, all necessary coefficients $g_{l'lm}(R)$ for a constant magnetic quantum number m can be computed by means of (13) and (14) provided that the initial values $g_{mlm}(R)$ are known. For $m = 0$ these quantities can be calculated directly from equation (8)

$$g_{0,l,0}(R) = \sqrt{2l+1}\, h_l(kR). \tag{16}$$

With the help of

$$(1 - x^2)\frac{\mathrm{d}}{\mathrm{d}x}P_l^m(x) = -lxP_l^m(x) + (l+m)P_{l-1}^m(x), \tag{17}$$

$$xP_l^m(x) - P_{l-1}^m(x) = (l - m + 1)\sqrt{1 - x^2}\,P_l^{m-1}(x) \tag{18}$$

and (12), one gets for $m \geqslant 1$

$$\frac{\mathrm{d}}{\mathrm{d}x}(P_m^m(x)P_l^m(x)) = -(l+m)(l-m+1)(2m-1)P_{m-1}^{m-1}(x)P_l^{m-1}(x) \tag{19}$$

and

$$\frac{\mathrm{d}}{\mathrm{d}x}(P_{l+1}(x) - P_{l-1}(x)) = (2l+1)P_l(x). \tag{20}$$

Integration by parts using (19) and (20) gives (for $m \geqslant 1$)

$$\int_{-1}^{+1} \mathrm{d}\zeta\, P_m^m(\zeta)P_l^m(\zeta)P_{l''}(\zeta) = \frac{(l+m)(l-m+1)(2m-1)}{(2l''+1)}$$

$$\times \int_{-1}^{+1} \mathrm{d}\zeta\, P_{m-1}^{m-1}(\zeta)P_l^{m-1}(\zeta)(P_{l''+1}(\zeta) - P_{l''-1}(\zeta)). \tag{21}$$

This result and the recursion formula for the spherical Hankel functions

$$h_{l-1}(x) + h_{l+1}(x) = (2l+1)h_l(x)/x \tag{22}$$

can be used to verify for $m \geqslant 0$

$$g_{m+1,l,m+1}(R) = \sqrt{\frac{2m+3}{2m+2}}\frac{\sqrt{(l+m+1)(l-m)}}{kR}g_{m,l,m}(R). \tag{23}$$

Now the system of recurrence relations is complete: equation (16) is used to generate the initial values for $m = 0$ and then equation (23) provides the initial values for $m > 0$.

Starting from these results all other coefficients can be computed by means of (14) and (13), for which m is constant. The total computational effort for the recursive construction of the $g_{l'lm}(R)$ needed in (7) is proportional to $l_{\max}^2 M$.

The upper limit $l_{\max}$ of the angular momenta which must be included in the expansion (3) or (7) can be estimated from a quasi-classical picture to be roughly

$$l_{\max}(l_{\max}+1) \approx k^2 R_{\text{pot}}^2 \tag{24}$$

where R_{pot} is the radius of the scattering potential. For non-overlapping potentials we have $R \geqslant 2R_{\text{pot}}$ and obtain for the prefactor in (23)

$$\sqrt{\frac{2m+3}{2m+2}}\frac{\sqrt{(l+m+1)(l-m)}}{kR} \leqslant \sqrt{\frac{3}{2}}\frac{\sqrt{l(l+1)}}{kR} \leqslant \sqrt{\frac{3}{8}}. \tag{25}$$

Therefore the absolute value of $g_{m+1,l,m+1}(R)$ is much smaller than the absolute value of $g_{m,l,m}(R)$. This property of the initial values propagates through all results of the recursion on a constant magnetic quantum number level (13, 14) and makes the truncation of the q_i sums in (7) possible. Furthermore it can be seen from equation (23) that the errors caused by such an approximation decrease considerably with the distance R. Therefore a great number of large-distance scattering processes, which occur in cluster calculations, can be computed with very low values for the truncation parameter M.

2.3. *Comparison with the* TSMQNE

Similar ideas as described above were realized in the Taylor-series magnetic quantum number expansion (TSMQNE) of Barton and Shirley [11, 12]. In order to compare both methods we express the $g_{l'lm}(R)$ for $m \geqslant 0$ by quantities introduced in [11]:

$$g_{l'lm}(R) = 4\pi\, \mathrm{i}^{l'-l} N_{lm} N_{l'm} h_0(kR) \sum_{p=0}^{l-m} C_{pm}^{l} H_{l'}^{pm}(kR). \tag{26}$$

The definition of the C_{pm}^{l} and recurrence relations for the $H_{l'}^{pm}(kR)$ can be found in [11]. In the TSMQNE the summation over the magnetic quantum numbers q_i in (7) is restricted to $-\tau \leqslant q_i \leqslant \tau$ in the same way as discussed above. But additionally the p summation in (26) is truncated by the condition $0 \leqslant p \leqslant \tau - m$. It is exactly this second step which is the weak point in the TSMQNE, because this approximation is not valid for small distances R. Using the results of [11] the summands in (26) may be written as

$$C_{pm}^{l} H_{l'}^{pm}(kR) = (-1)^m \frac{(l'+m)!}{(l'-m)!}\frac{(l+m+p)!}{(l-m-p)!}\frac{1}{p!(p+m)!} \times \sum_{t=0}^{l} \frac{(l'+t)!}{t!(l'-t)!}\frac{(t+p+m)!}{(t+m)!}\left(\frac{\mathrm{i}}{2kR}\right)^{t+p+m}. \tag{27}$$

From this formal expression (27) it follows that truncating the p sum requires $l^2 \ll kR$. This is just the same condition under which spherical Hankel functions can be approximated by their asymptotic values [19]. But this requirement is not fulfilled for close-packed clusters of atoms. From the discussion above it is clear that only $l \ll kR$ is realized for nearest neighbours. Therefore a truncation of the p sum in (26) leads to errors in the coefficients $g_{l'lm}(R)$ which increase considerably with the angular momentum l. Furthermore this approximation breaks the symmetry (10) of the $g_{l'lm}(R)$. In the TSMQNE

the t sum, which is closely related to the angular momentum of the scatterer l', is fully included, whereas the p sum, which is connected with the angular momentum at the emitter l, is restricted to low values. Therefore the TSMQNE can be applied preferentially for scattering events of spherical waves having low angular momenta with respect to the emitter. For reliable multiple-scattering calculations this doubtful approximation should be avoided and the full p sum has to be taken over the whole range from 0 to $l - m$. Then the computational effort for a recursive calculation of the $H_{l'}^{pm}(kR)$ is proportional to $l_{\max}^2 \tau = l_{\max}^2 M$ and the involved recursion scheme of the TSMQNE has no advantages over the more direct one for the $g_{l'lm}(R)$, presented in the preceding section.

2.4. *Instrumental angular broadening*

The finite angular resolution of the detector in the experimental apparatus can have a considerable influence on the measured intensity anisotropies [21, 22]. In order to include this angular broadening effect in the theory we have to integrate the intensity $I(\boldsymbol{K}, E)$, given by (1)–(3), over a conical range of wavevectors $\boldsymbol{K}$ around the detector axis $\boldsymbol{K}_0$. Deformations of the cone due to the refraction of the outgoing waves at the surface potential step can be neglected. Then the problem consists in evaluating the following mixed quadratic terms in the expression for the intensity (equations (1)–(3))

$$Q = \int \mathrm{d}\Omega_k \, \mathrm{e}^{\mathrm{i}\boldsymbol{k}\cdot(\boldsymbol{R}'-\boldsymbol{R})} Y_{L'}^*(\boldsymbol{k}) Y_L(\boldsymbol{k}). \tag{28}$$

In the following discussion it is assumed that the z axis of the coordinate system points to the image of the centre of the detector opening:

$$\boldsymbol{k}_0 = k\boldsymbol{e}_z. \tag{29}$$

Using

$$\boldsymbol{k} = k \sin\theta(\cos\varphi\, \boldsymbol{e}_x + \sin\varphi\, \boldsymbol{e}_y) + k\cos\theta \boldsymbol{e}_z \tag{30}$$

$$\boldsymbol{R}_\perp = R \sin\theta_{\boldsymbol{R}}(\cos\varphi_{\boldsymbol{R}} \boldsymbol{e}_x + \sin\varphi_{\boldsymbol{R}} \boldsymbol{e}_y) \tag{31}$$

Q becomes

$$Q = \int_0^\alpha \mathrm{d}\theta \sin\theta \int_0^{2\pi} \mathrm{d}\varphi\; Y_{L'}^*(\theta, \varphi) Y_L(\theta, \varphi)$$
$$\times \exp[\mathrm{i}\boldsymbol{k}_0 \cdot (\boldsymbol{R}' - \boldsymbol{R}) \cos\theta + \mathrm{i}\, k |\boldsymbol{R}'_\perp - \boldsymbol{R}_\perp| \sin\theta \cos(\varphi - \varphi_0)] \tag{32}$$

where α is the half-angle of the conical aperture. The essential effects of the finite angular resolution are caused by the phase factor in (32), in which the products of wave numbers and distances can be much larger than one for many scattering pathways. Neglecting terms of higher order in the small parameter θ one obtains

$$Q = \mathrm{e}^{\mathrm{i}\boldsymbol{k}_0\cdot(\boldsymbol{R}'-\boldsymbol{R})} Y_{L'}^*(\boldsymbol{k}_0) Y_L(\boldsymbol{k}_0) \pi\alpha^2 a(\alpha k |\boldsymbol{R}'_\perp - \boldsymbol{R}_\perp|) \tag{33}$$

where $\pi\alpha^2$ is the aperture area and

$$a(x) = (2/x) J_1(x) \tag{34}$$

is an aperture attenuation function. This result was previously derived and discussed in [21], but it was applied only for mixed terms in the quadratic form of the intensity (equations (1)–(3)) in which at least one factor is the direct wave. In these cases one of

the vectors $\boldsymbol{R}$ or $\boldsymbol{R}'$ is the emitter position and the aperture attenuation can be described by a single factor for each scattering pathway.

In the general case the attenuation function $a(\alpha k|\boldsymbol{R}'_\perp - \boldsymbol{R}_\perp|)$ depends on two positions $\boldsymbol{R}$ and $\boldsymbol{R}'$, which are the final atoms of two independent scattering pathways. Therefore the integrated intensity is a sum over all possible pairs of scattering pathways. Such a representation is very cumbersome for numerical calculations. With the help of Gegenbauer's addition theorem for Bessel functions [19]

$$\frac{J_1(|\boldsymbol{R}'_\perp - \boldsymbol{R}_\perp|)}{|\boldsymbol{R}'_\perp - \boldsymbol{R}_\perp|} = 2\sum_{\lambda=0}^{\infty}(\lambda+1)\frac{J_{\lambda+1}(R'_\perp)}{R'_\perp}\frac{J_{\lambda+1}(R_\perp)}{R_\perp}C_\lambda^{(1)}[\cos(\varphi_{R'}-\varphi_R)] \tag{35}$$

and the addition theorem for the Gegenbauer polynomials (ultraspherical polynomials) [23, 24]

$$C_\lambda^{(1)}[\cos(\varphi_{R'}-\varphi_R)] = \sum_{\mu=0}^{\lambda} 4^\mu(2\mu+1)\frac{(\lambda-\mu)!(\mu!)^2}{(\lambda+\mu+1)!} \times (\sin\varphi_{R'})^\mu C_{\lambda-\mu}^{(\mu+1)}(\cos\varphi_{R'})(\sin\varphi_R)^\mu C_{\lambda-\mu}^{(\mu+1)}(\cos\varphi_R) \tag{36}$$

the attenuation function $a(\alpha k|\boldsymbol{R}'_\perp - \boldsymbol{R}_\perp|)$ can be factorized. Then the total intensity is given by

$$\bar{I}(\boldsymbol{K}_0, E) \sim \sum_{\boldsymbol{R}_0}\sum_{m_0}\sum_{\lambda=0}^{\infty}\sum_{\mu=0}^{\lambda}\left|\sum_{l_0} M_{L_0}(E)B_{L_0}^{(\lambda,\mu)}(\boldsymbol{k}_0, \boldsymbol{R}_0)\right|^2 \tag{37}$$

$$\begin{aligned} B_{L_0}^{(\lambda,\mu)}(\boldsymbol{k}_0, \boldsymbol{R}_0) &= A_{L_0}^{(0)}(\boldsymbol{k}_0, \boldsymbol{R}_0) \\ &+ \sum_{\boldsymbol{R}_1}{}' \, \mathrm{e}^{-\mathrm{i}\boldsymbol{k}_0(\boldsymbol{R}_1-\boldsymbol{R}_0)} F_{\lambda\mu}(\boldsymbol{R}_1-\boldsymbol{R}_0)A_{L_0}^{(1)}(\boldsymbol{k}_0, \boldsymbol{R}_1, \boldsymbol{R}_0) \\ &+ \sum_{\boldsymbol{R}_1}{}' \sum_{\boldsymbol{R}_2}{}' \, \mathrm{e}^{-\mathrm{i}\boldsymbol{k}_0(\boldsymbol{R}_2-\boldsymbol{R}_0)} F_{\lambda\mu}(\boldsymbol{R}_2-\boldsymbol{R}_0)A_{L_0}^{(2)}(\boldsymbol{k}_0, \boldsymbol{R}_2\,\boldsymbol{R}_1, \boldsymbol{R}_0) + \ldots \end{aligned} \tag{38}$$

with (7) and

$$F_{\lambda\mu}(\boldsymbol{R}) = 2^\mu\mu!\sqrt{\frac{(2\mu+1)(\lambda-\mu)!}{(\lambda+1)(\lambda+\mu+1)!}}[J_\lambda(\alpha kR_\perp)+J_{\lambda+2}(\alpha kR_\perp)] \times (\sin\varphi_R)^\mu C_{\lambda-\mu}^{(\mu+1)}(\cos\varphi_R). \tag{39}$$

The new summation indices λ and $\mu \leqslant \lambda$ can be restricted to low values because the Bessel functions with positive order n decrease according to $J_n(x) \leqslant (x/2)^n/n!$ [19]. The Gegenbauer polynomials needed in (39) can be calculated from [19]

$$(n+1)C_{n+1}^{(m)}(x) = 2(n+m)xC_n^{(m)}(x) - (n+2m-1)C_{n-1}^{(m)}(x) \tag{40}$$

with $C_0^{(m)}(x) = 1$ and $C_1^{(m)}(x) = 2mx$.

3. Angle-resolved $M_{23}VV$ AES from Ni(111)

The most delicate input parameters for the theory described above are the transition matrix elements, because *ab initio* calculations within a full many-particle treatment were hardly possible until now. However, fortunately, a lot of practical work has been

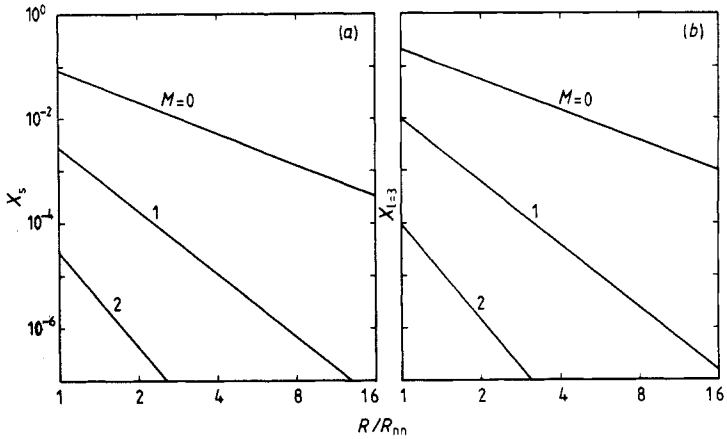

Figure 1. (*a*) Relative error for the scattering of a scattered wave (defined in [10]) as a function of the truncation parameter M and the distance R (in units of the nearest-neighbour distance R_{nn}), $E = 56.9$ eV. (*b*) Relative error for the first scattering process of the excited electrons with the angular momentum $l = 3$ as in (*a*).

performed for the $M_{23}VV$ Auger transition in nickel. Calculations for nickel atoms within a one-electron picture [25] yield the result that the probability of transitions in final states with angular momentum $l_0 = 3$ is larger by a factor of 100 than that for all other transitions. This statement was confirmed in [26]. Therefore we make use of the approximation

$$M_{L_0}(E) = \delta_{l_0,3} \tag{41}$$

in the expression for the Auger intensity (37). This assumption has already proved its worth in previous investigations of angle-resolved Auger spectra from a Ni(001) surface [25–29] and a Ni(110) surface [30, 31].

The number of emitter positions and scattering pathways which contribute to the intensity is mainly determined by the inelastic mean free path of the electrons, for which a value of 4.72 Å [32] was used. We have calculated contributions from more than 5000 single-, double- and triple-scattering pathways starting from all different emitter positions in the eight upper layers. An instrumental broadening with $\alpha = 3°$ was included. The scattering properties of the atoms were described by ten complex scattering phase shifts, which take into account uncorrelated isotropic thermal vibrations of the atoms with a mean square displacement of 0.0043 Å^2 [33].

Figure 1 illustrates that very small values for the truncation parameter M can guarantee a high accuracy of the multiple-scattering calculations in the energy range of interest. The definitions of the error parameters used in figure 1 can be found in [10].

In figures 2, 3 and 4 the calculated Auger electron distributions for the three main azimuths are compared with the experimental data from [16]. The measurements were performed with the help of a three-grid LEED–AES system, in which an immovable collector was placed behind a small hole in the fluorescent screen of the LEED optics, while the electron gun was rotated together with the sample.

The general shape of the theoretical spectra is in good qualitative agreement with the measured curves. But this impression is impaired by systematic deviations of the calculated peak positions from the experimental ones. Most obviously these angular

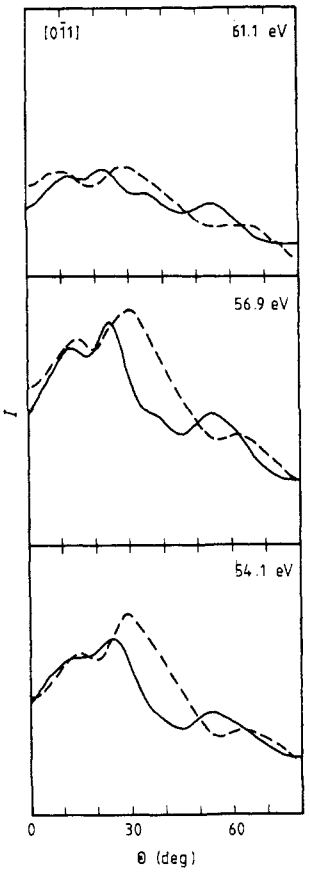

Figure 2. $M_{23}VV$ Auger electron intensity (in arbitrary units) from a clean Ni(111) surface as a function of the polar angle Θ for the [0$\bar{1}$1] azimuth: Full multiple-scattering calculation (full curve) and experimental results from [16] (broken curve).

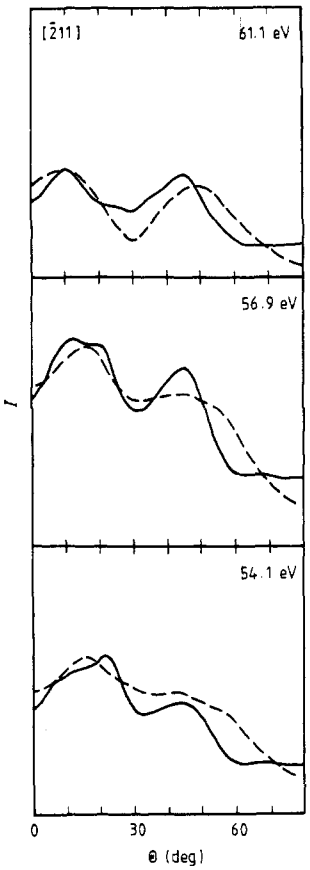

Figure 3. $M_{23}VV$ Auger electron intensity as in figure 2 for the [$\bar{2}$11] azimuth.

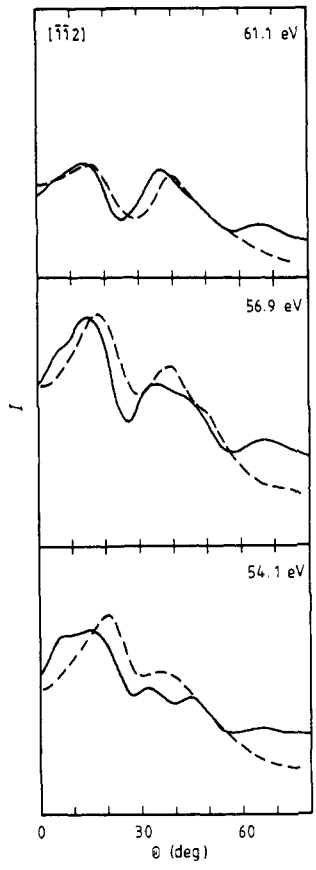

Figure 4. $M_{23}VV$ Auger electron intensity as in figure 2 for the [1$\bar{1}$2] azimuth.

shifts can be seen in the spectra for the [0$\bar{1}$1] azimuth. These differences cannot be removed either by increasing the height of the surface potential step within realistic limits or by relaxation of the surface layers with changes of the interlayer spacings in the order of magnitude proposed by theoretical investigations [34] or LEED measurements [32]. In this comparison between theory and experiment one should take into consideration that some uncertainties exist in the experimental data concerning the zero point in the angular scale, because the spectra can be shifted by magnetic fields in the vacuum chamber. In particular we have no symmetries in the spectra of the [$\bar{2}$11] azimuth and the [1$\bar{1}$2] azimuth which allow control of the position of the surface normal.

It must be concluded that the high-quality multiple-scattering calculations have not answered all the questions. We have checked carefully that higher-order-scattering

contributions are negligible in the example presented and we can be sure that the elastic scattering effects of the excited Auger electrons were treated exactly. Remaining differences between experiment and theory must be addressed to other origins. The weak point in the theory is undoubtedly the approximation for the Auger transition matrix elements (41), which assumes an equal weight for all magnetic quantum numbers m_0. This is quite reasonable for atoms in an isotropic or close-packed surroundings, but it is questionable for atoms at the surface. Therefore the transition matrix elements should be studied more carefully starting from a surface band structure calculation which takes into account the effects of a lower symmetry at the surface. From an experimental point of view the rather large background of secondary electrons, which was subtracted from the raw data in order to obtain the intensity of the $M_{23}VV$ Auger electrons [25, 29], is troublesome. We cannot definitely exclude the possibility that small anisotropies in the background of the inelastically scattered electrons have falsified the extracted angle-resolved Auger electron spectra. The degree of correspondence between experiment and theory achieved for the (111) surface (present paper), the (001) surface [29] and the (110) surface [31] makes it difficult to use the diffraction of $M_{23}VV$ Auger electrons in nickel for structure investigations of more complicated surfaces, e.g. covered with adsorbates.

Acknowledgments

The author is grateful to Dr A Chassé (Martin-Luther-University Halle/Wittenberg) for providing the scattering phase shifts, to Professor S Mróz (University of Wroclaw) for communicating the experimental results prior to publication, and to Professor P Ziesche (Technical University Dresden) for his steady interest and support of this work.

Appendix

The rotation matrices $D^{(l)}_{m'm}(\boldsymbol{a}_2, \boldsymbol{a}_1)$ transform spherical harmonics from a coordinate system with the z axis $\boldsymbol{a}_1$ into a coordinate system with the z axis $\boldsymbol{a}_2$. If θ_i and φ_i are the angular coordinates of $\boldsymbol{a}_i$ in the basis system spanned by the unity vectors $\boldsymbol{e}_x$, $\boldsymbol{e}_y$ and $\boldsymbol{e}_z$,

$$\boldsymbol{a}_i = a_i(\sin\theta_i(\cos\varphi_i\,\boldsymbol{e}_x + \sin\varphi_i\,\boldsymbol{e}_y) + \cos\theta_i\,\boldsymbol{e}_z) \tag{A1}$$

one obtains

$$D^{(l)}_{m'm}(\boldsymbol{a}_2, \boldsymbol{a}_1) = \mathrm{e}^{\mathrm{i}m'\gamma + \mathrm{i}m\alpha} d^{(l)}_{m'm}(\beta) \tag{A2}$$

where α, β and γ are the Eulerian angles, which can be calculated from

$$\begin{aligned}
\cos\beta &= \sin\theta_2 \sin\theta_1 \cos(\varphi_2 - \varphi_1) + \cos\theta_2 \cos\theta_1 \\
\sin\alpha \sin\beta &= \sin\theta_2 \sin(\varphi_2 - \varphi_1) \\
\cos\alpha \sin\beta &= \sin\theta_2 \cos\theta_1 \cos(\varphi_2 - \varphi_1) - \cos\theta_2 \sin\theta_1 \\
\sin\gamma \sin\beta &= -\sin\theta_1 \sin(\varphi_2 - \varphi_1) \\
\cos\gamma \sin\beta &= -\cos\theta_2 \sin\theta_1 \cos(\varphi_2 - \varphi_1) + \sin\theta_2 \cos\theta_1 .
\end{aligned} \tag{A3}$$

The $d^{(l)}_{m'm}(\beta)$ are determined by

$$d^{(l)}_{m'm}(\beta) = \left(\frac{(l+m')!\,(l-m')!}{(l+m)!\,(l-m)!}\right)^{1/2} (\cos(\beta/2))^{m'+m} \times (\sin(\beta/2))^{m'-m}\, P^{(m'-m,m'+m)}_{l-m'}(\cos\beta), \tag{A4}$$

where $P^{(m,n)}_{l}(x)$ are the Jacobi polynomials [19]. The $d^{(l)}_{m'm}(\beta)$ obey the symmetry relations

$$d^{(l)}_{m',m}(\beta) = d^{(l)}_{-m,-m'}(\beta) \tag{A5}$$

$$d^{(l)}_{m',m}(\beta) = (-1)^{m+m'} d^{(l)}_{m,m'}(\beta) \tag{A6}$$

and can be calculated for $m' \geqslant 0$ and $|m| \leqslant m'$ by means of the following recurrence relations:

$$b_{l+1,m} b_{l+1,m'} d^{(l+1)}_{m'm}(\beta) = (2l+1)[(l+1)\cos\beta - mm'/l] d^{(l)}_{m'm}(\beta) - [(l+1)/l] b_{l,m} b_{l,m'} d^{(l-1)}_{m'm}(\beta) \tag{A7}$$

with

$$b_{l,m} = \sqrt{l^2 - m^2} \tag{A8}$$

and the initial values

$$d^{(m')}_{m'm}(\beta) = 2^{-m'} \left(\frac{(2m')!}{(m'+m)!\,(m'-m)!}(1+\cos\beta)^{m'+m}(1-\cos\beta)^{m'-m}\right)^{1/2} \tag{A9}$$

and

$$d^{(m'+1)}_{m'm}(\beta) = \left(\frac{2m'+1}{(m'+m+1)(m'-m+1)}\right)^{1/2} [(m'+1)\cos\beta - m] d^{(m')}_{m'm}(\beta). \tag{A10}$$

References

[1] Pendry J B 1975 *J. Phys. C: Solid State Phys.* **8** 2413–22
[2] Holland B W 1975 *J. Phys. C: Solid State Phys.* **8** 2679–87
[3] Aberdam D, Baudoing R, Blanc E and Gaubert C 1976 *Surf. Sci.* **57** 306–22
[4] Davis H L and Kaplan T 1976 *Solid State Commun.* **19** 595–7
[5] Weeks S P and Liebsch A 1977 *Surf. Sci.* **62** 197–205
[6] Lindsay R N and Kinniburgh C G 1977 *Surf. Sci.* **63** 162–73
[7] Barton J J and Shirley D A 1985 *Phys. Rev.* B **32** 1892–905
[8] Poon H C, Snider D and Tong S Y 1986 *Phys. Rev.* B **33** 2198–206
[9] Fritzsche V and Rennert P 1986 *Phys. Status Solidi* b **135** 49–60
[10] Fritzsche V 1989 *Surf. Sci.* **213** 648–56
[11] Barton J J and Shirley D A 1985 *Phys. Rev.* A **32** 1019–26
[12] Barton J J and Shirley D A 1985 *Phys. Rev.* B **32** 1906–20
[13] Rehr J J, Albers R C, Natoli C R and Stern E A 1986 *Phys. Rev.* B **34** 4350–3
[14] Fritzsche V 1988 *Phys. Status Solidi* b **147** 485–94
[15] Fritzsche V 1990 *J. Phys.: Condens. Matter* **2** 1413–24
[16] Mróz S and Stachnik B 1989 *Proc. XIth Int. Vac. Congr. and 7th Int. Conf. Solid Surfaces* (*Cologne*) at press
[17] Holland B W 1971 *Surf. Sci.* **28** 258–66
[18] Jepsen D W, Marcus P M and Jona F 1972 *Phys. Rev.* B **5** 3933–52

[19] Abramowitz M and Stegun I A (ed) 1965 *Handbook of Mathematical Functions* (New York: Dover)
[20] Fritzsche V and Rennert P 1984 *Proc. 14th Symp. Electronic Structure* ed P Ziesche (Dresden: Technical University) pp 77–81
[21] Barton J J, Robey S W and Shirley D A 1986 *Phys. Rev.* B **34** 778–91
[22] Sagurton M, Bullock E L and Fadley C S 1987 *Surf. Sci.* **182** 287–361
[23] Ryshik I M and Gradstein I S 1957 *Tables of Series, Products and Integrals* (Berlin: Deutscher Verlag Wissenschaften) p 373
[24] Whittaker E T and Watson G N 1952 *A Course of Modern Analysis* (Cambridge: Cambridge University Press) p 335
[25] Aberdam D, Baudoing R, Blanc E and Gaubert C 1978 *Surf. Sci.* **71** 279–305
[26] Aschenbach J 1986 *PhD Thesis* Technical University Clausthal
[27] Plociennik J M, Barbet A and Mathey L 1981 *Surf. Sci.* **102** 282–94
[28] Fritzsche V and Rennert P 1986 *Acta Universitatis Wratislaviensis* **937** 59–67 (Proc. 9th Seminar on Surface Physics)
[29] Mróz S, Mróz A, Wieczorek A and Fritzsche V 1989 *Surf. Sci.* **224** 243–9
[30] Baudoing R, Blanc E, Gaubert C, Gauthier Y and Gnuchev N 1983 *Surf. Sci.* **128** 22–36
[31] Fritzsche V, Chassé A and Mróz S 1990 *Surf. Sci.* **231** 59–63
[32] Demuth J E, Marcus P M and Jepsen D W 1975 *Phys. Rev.* B **11** 1460–74
[33] Singh N and Sharma P K 1971 *Phys. Rev.* B **3** 1141–7
[34] Ning Ting, Yu Qingliang and Ye Yiying 1988 *Surf. Sci.* **206** L857–63